Western Region Technical Attachment
No. 89-18
July 11, 1989

THE POLEWARD BOUNDARY OF JET STREAM CIRRUS SHIELDS

[Editor's Note: The following Technical Attachment (TA) is a summary of a paper by Dale Durran and Daniel Weber from the March 1988 issue of the *Monthly Weather Review.* This excellent paper has operational applications and interested readers should consult the reference at the end of this TA for more detailed information.]

Ever since satellite imagery has been available to forecasters, large cirrus shields with sharp poleward boundaries have been identified with the jet stream. Typically, the jet stream is positioned just north of the poleward boundary. The two most common hypotheses suggest that either the cirrus clouds are formed as the result of differential vertical motion on each side of the jet stream or that the cirrus boundary results from differences in the humidity field. The former has been most commonly accepted.

It has been generally believed that secondary circulations at the jet entrance and exit region (Figure 1) are responsible for generating the differential vertical motion fields. Clouds which form in the ascending air in the anticyclonic-shear portion of the entrance region would be advected along the equatorward side of the jet, forming a band of cirrus. Conversely, the downward motion in the cyclonic-shear portion of the entrance region would inhibit cloud development on the poleward side of the jet. However, other studies have shown that the advection of the pre-existing moisture field may be the primary generator of the cirrus band and that differential vertical motion plays only a secondary role.

Durran and Weber (1988), examined three cases to determine the physical processes that produce the cirrus boundary. The case studies were selected from data gathered during the First GARP (Global Atmosphere Research Program) Global Experiment (FGGE). The data consisted of analyses prepared by the European Centre for Medium Range Weather Forecasts (ECMWF). A cloud model was then employed to generate cloud fields. In each case, the humidity and temperature fields were initialized with 0000 UTC or 1200 UTC data and integrated forward through 24 hours. The winds were linearly interpolated between the grid data at the middle time, and beginning or end of the 24 hour period. By 24 hours, the clouds were completely initialized by the model. Further changes in the cloud field were associated with the dynamics of the evolving weather pattern.

Durran and Weber were uncertain about the initial humidity field in the ECMWF data, so they decided to assess their model by comparing initialized FGGE humidity fields with a "controlled" field in which the humidity was initialized everywhere at 80%. The time-dependent vertical velocity fields were identical in both cases; only the initialized humidity fields differed. The resulting 400 mb cloud patterns are shown in Figure 2 at 12 and 24 hours. After 24 hours there is not much difference in the cloud fields. This example emphasizes how dependent the synoptic cloud and precipitation patterns are upon the vertical velocity fields. This example also illustrates that even with a poor initial humidity analysis, a numerical model is very efficient in correcting the situation within 12-24 hours.

Since the results of the three case studies by Durran and Weber were similar, only one will be presented here. They verified their model-generated cloud fields with satellite imagery. Since they felt that the model-generated 400 mb cloud fields best represented the cirrus shield south of the jet stream, this level was used for comparison in all their cases.

Figure 3 is an enhanced satellite image from 1200 UTC March 11, 1979, while the cloud field generated by the model is shown in Figure 4. The model clouds correlate quite well with the first level of enhancement of the satellite image, suggesting that the FGGE data and the model adequately represent the circulation responsible for the cloud field. Figures 5a and 5b represent the corresponding 300 mb horizontal wind speed and 400 mb vertical velocity generated by the model at 0000 UTC March 11, 1979. This is the mid-point of the 24-hour run. The heavy black line represents portions of the 300 mb wind speed that exceed 45 ms-1. Note that the vertical motion fields at the entrance and exit regions of the jet are similar to those presented in classical theory. However, Figure 5b does not support the idea that the sharp cirrus boundary is produced by a differential vertical motion field. In this case, the area of strongest upward vertical motion is actually north of the jet. In the two other cases researched by Durran and Weber, the strongest vertical motion was south of the jet, yet in each case there was also significant upward motion on the north side. Therefore, even though there is evidence that the cloudiness equatorward of the jet may be produced by vertical motions, there is no support for subsidence poleward of the jet to explain the cloud free area.

In order to better understand the kinematics of these cases, Durran and Weber investigated the trajectories of the air parcels near the cloud boundary to determine their upstream locations at the beginning of the 24 hour simulation. Figures 6a and 6b show the upstream trajectories computed from two different regions along the cloud boundary for the case discussed above. Figure 6a corresponds to the first 12 hours of the model run, while 6b corresponds to the second 12 hours. In each figure, the trajectory ends at 400 mb. The two numbers plotted at the beginning of each trajectory indicate the parcel's original pressure (top) and the saturation deficit (bottom). The saturation deficit is defined as the amount of vertical motion (mb) that the parcel must undergo to reach saturation. The tens digit of the pressure level of the parcel is plotted along the trajectory to show vertical motion.

In Figure 6a, it is obvious that air arriving at the cloud boundary has undergone a fair amount of horizontal confluence during the first 12 hours of the model run. The air parcel trajectory just to the north of the cloud boundary is lifted 38 mb but the saturation deficit is 121 mb. There is little vertical motion associated with the trajectories further north and their saturation deficits indicate a relatively dry source region. The three remaining trajectories, along and south of the cloud boundary, have low saturation deficits and undergo significant lifting, resulting in the saturation of the air parcel.

During the second 12 hours of the model run (figure 6b), all trajectories undergo significant lifting; however, only those associated with the drier air upstream (northern most trajectories) remain unsaturated. It should be noted that the vertical lifting was not uniform among the upstream air parcels; those that ended up along or south of the cloud boundary underwent more ascent. However, it is noteworthy that there was significant upward motion in both the cloudy region and in the clear air. The resulting existence and position of the cloud edge is determined primarily by the pre-existing moisture gradient. The results were similar for the other two cases in this paper. Observed vertical motion was fairly uniform on both sides of the cloud boundary, and the pre-existing moisture gradient resulted in a cloud mass developing equatorward of the jet stream.

In conclusion, the cases studies by Durran and Weber suggest that differential vertical motions may play a secondary role in the initial generation of the moisture gradient associated with jet stream cirrus. This gradient may then become concentrated by horizontal confluence. Although there is significant upward vertical motion on both sides of the jet axis, the cirrus shield forms in the more moist air along and equatorward of the jet.

Reference:

Durran, D. R. and D. B. Weber, 1988: An Investigation of the Poleward Edges of Cirrus Clouds Associated with Mid-latitude Jet Streams. Mon. Wea. Rev., 116, 702-714.

[Editor's Note: This paper also suggests some important implications regarding the interpretation of water vapor imagery. Brightness values of the water vapor imagery depend on the amount and vertical distribution of moisture in the mid to upper levels of the troposphere. Distinct boundaries (often elongated dark bands) are found where there is significant convergence or strong subsidence throughout a deep layer of the troposphere. These dark boundaries are often associated with deformation zones or cold air advection (subsidence). Jet stream signatures in water vapor imagery, however, are often indistinct and are characterized by only somewhat darker, narrow channels with nearly equal brightness values poleward and equatorward of the jet axis. The Durran and Weber study helps explain why this occurs. Upward vertical motion on both sides of the jet axis increases the moisture at higher levels and leads to relatively higher brightness values in these regions. However, there is only sufficient moisture along and equatorward of the jet axis to produce clouds.]

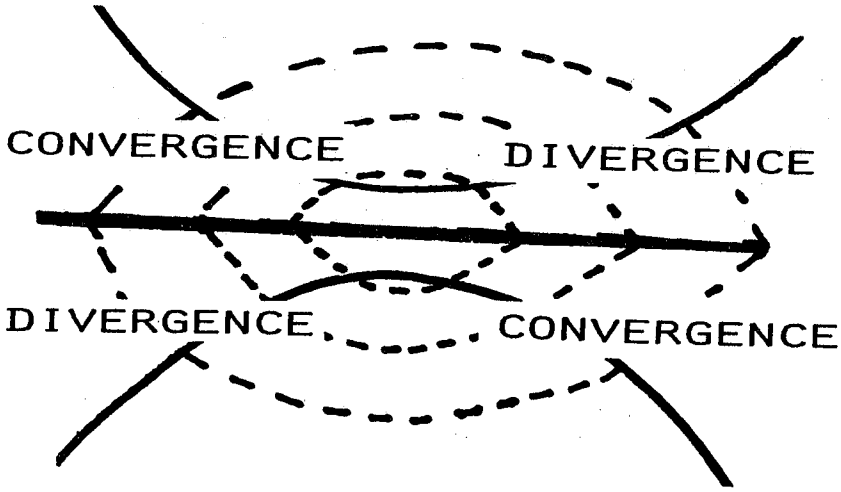

Figure 1

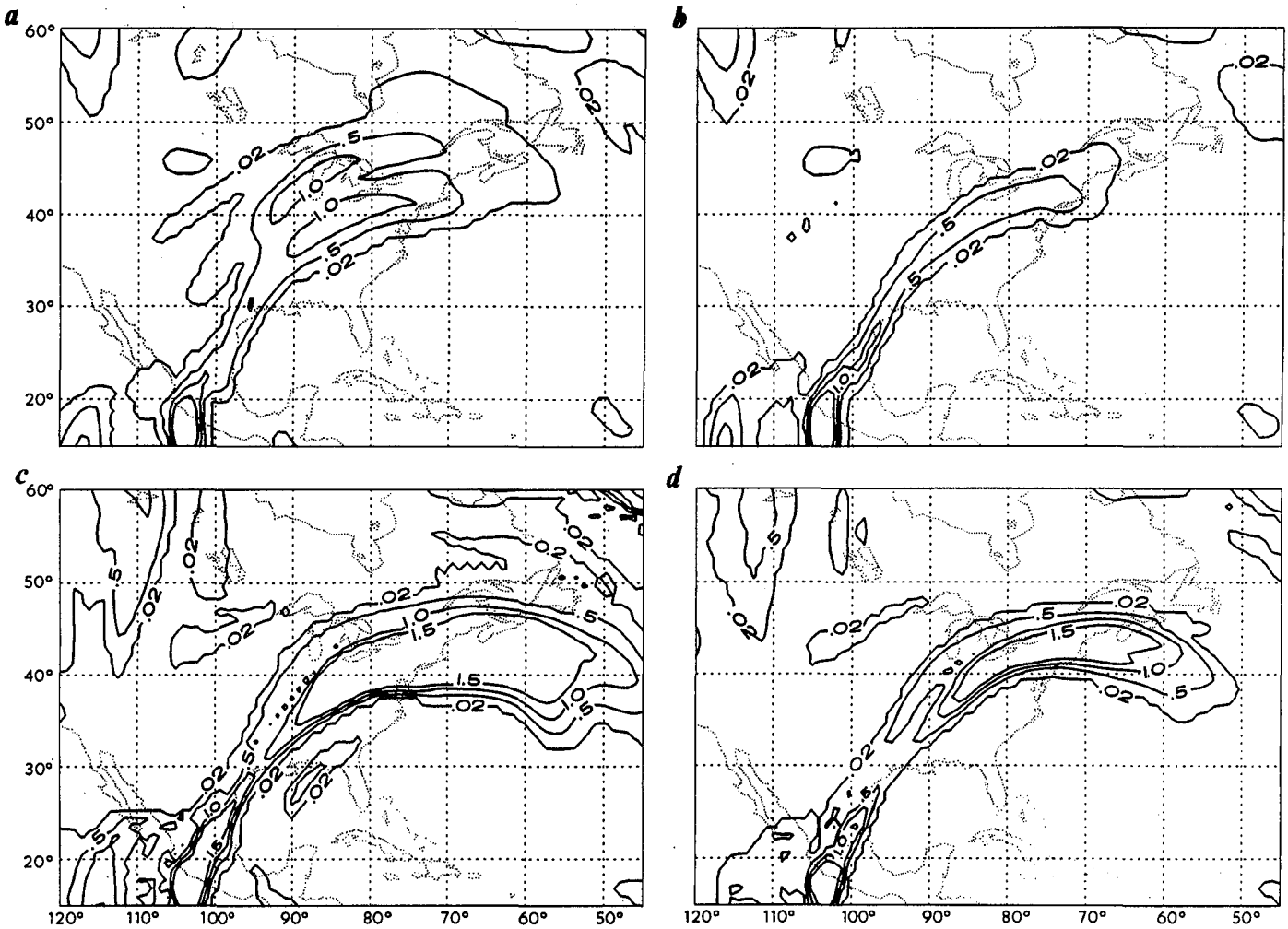

FIG. 2. Contours of the 400-mb cloud field in g kg^{-1} (a) after 12 hours with a uniform initial humidity of 80%; (b) after 12 hours with humidity initialized from ECMWF data; (c) after 24 hours with uniform initial humidity of 80%; (d) after 24 hours with humidity initialized from ECMWF data.

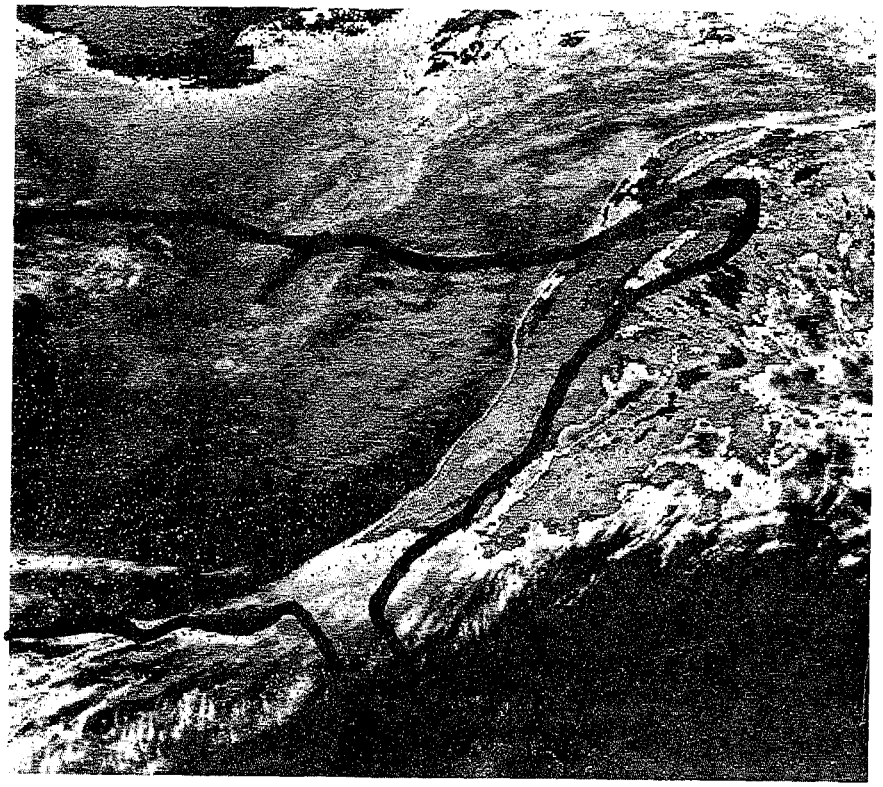

Figure 3 - 1200 UTC March 11, 1979

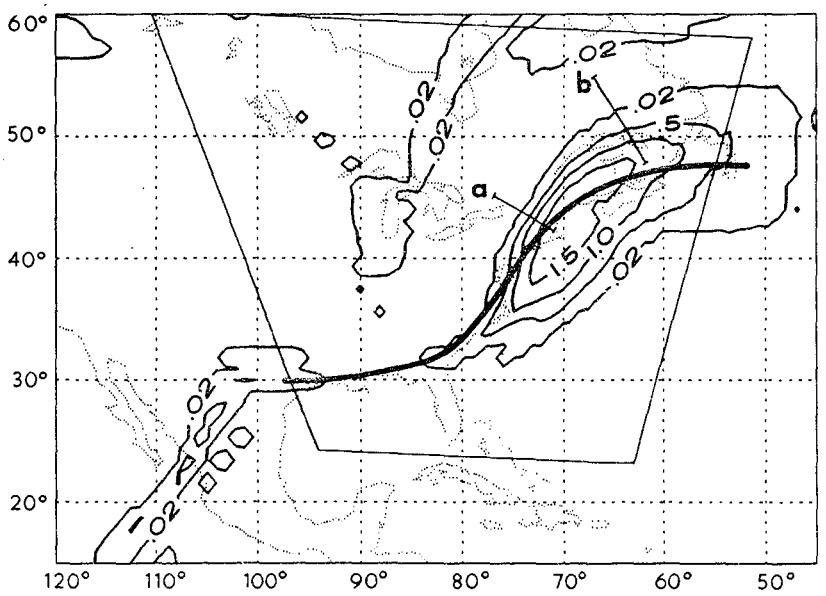

Figure 4 - Contours of 400 mb model-generated cloud field in gKg^{-1} at 1200 UTC March 11, 1979. The jet axis is indicated with a heavy line. Quadrilateral shows approximate area covered by satellite image. Short line segments show the location of the endpoints for trajectories shown in Figure 6.

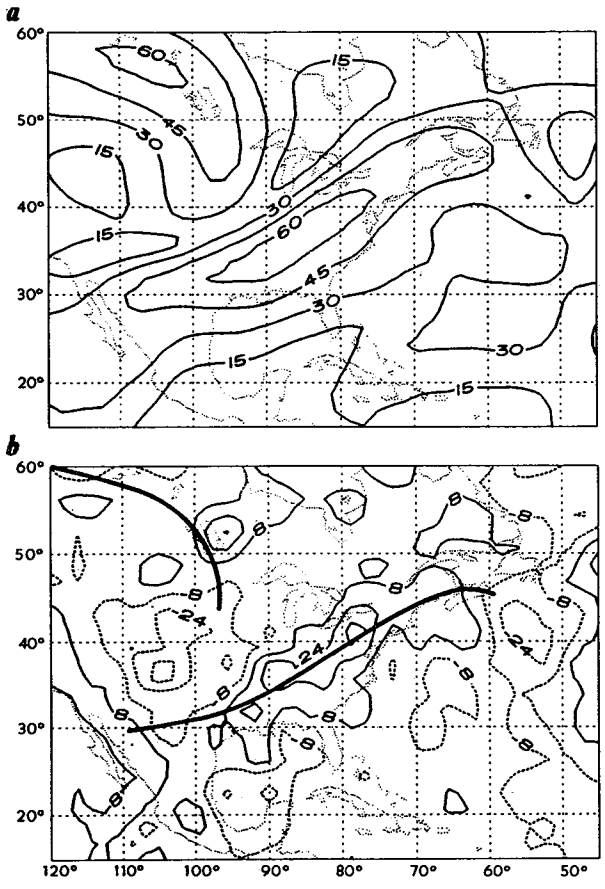

Figure 5 - Velocity fields at 0000 UTC March 11, 1979: (a) 300 mb horizontal windspeed, countour interval of 15ms^{-1}; (b) 400 mb vertical velocity, contour interval of 1.6 x 10^{-3} mb s^{-1}.

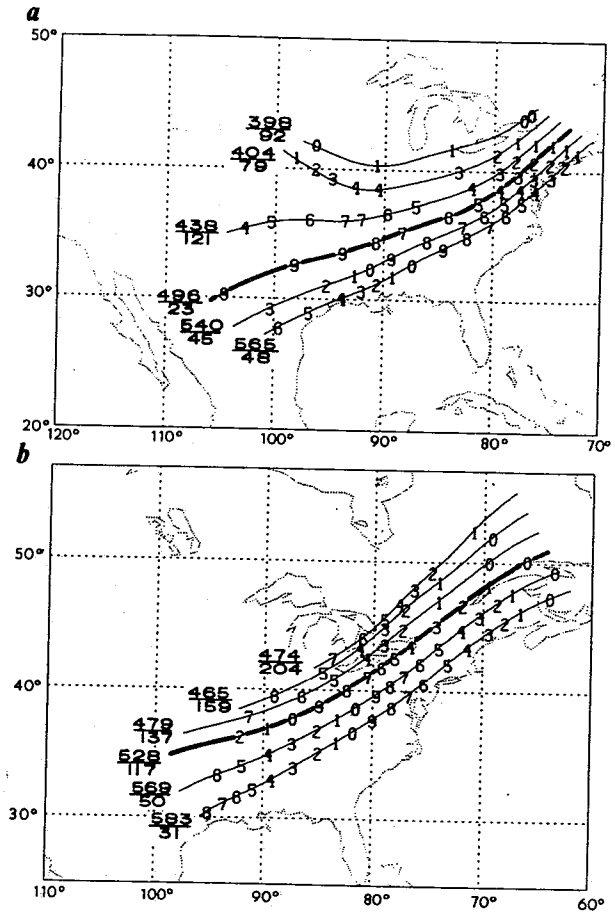

Figure 6 - Backwards trajectories from the vicinity of the cloud edge for the period 1200 UTC March 10 to 1200 UTC March 11, 1979. All trajectories terminate at 400 mb. The presure level and the saturation pressure deficit are plotted in mb at the upstream end of each trajectory.